An emerging PB2-627 polymorphism increases the pandemic potential of avian influenza virus by breaking through ANP32 host restriction in mammalian and avian hosts

Yuxin Guo[1], Sicheng Shu[1], Yong Zhou[1], Wenjing Peng[1], Zhimin Jiang[1], Yudong Li[1], Tian Li[1], Fanshu Du[1], Linlin Wang[1], Xue Chen[1], Jinze Dong[1], Chuankuo Zhao[1], Maggie Haitian Wang[2,3], Yipeng Sun[1], Honglei Sun[1], Lu Lu[4], Paul Digard[4], Kin-Chow Chang[5], Hui-Ling Yen[6], Jinhua. Liu[1*], Juan Pu[1*]

Affiliations:

[1] National key laboratory of Veterinary public health security, Key Laboratory for Prevention and Control of Avian Influenza and Other Major Poultry Diseases, Ministry of Agriculture and Rural Affairs, College of Veterinary Medicine, China Agricultural University; Beijing, China.

[2] Centre for Clinical Research and Biostatistics, JC School of Public Health and Primary Care, the Chinese University of Hong Kong, Hong Kong SAR, China.

[3] CUHK Shenzhen Research Institute, Shenzhen, China.

[4] The Roslin Institute, University of Edinburgh, Edinburgh, United Kingdom.

[5] School of Veterinary Medicine and Science, University of Nottingham, Sutton Bonington Campus, Loughborough, UK.

[6] School of Public Health, Li Ka Shing Faculty of Medicine, The University of Hong Kong, Hong Kong Special Administrative Region, China.

* Corresponding author. Email: Juan Pu: pujuan@cau.edu.cn; Jinhua Liu: ljh@cau.edu.cn.

Abstract

Alterations in the PB2-627 domain could substantially increase the risk of an avian influenza virus (AIV) pandemic. So far, a well-known mammalian mutation PB2-E627K has not been maintained in AIV in poultry, which limits the spread of AIVs from avian to humans. Here, we discovered a variant, PB2-627V, which combines the properties of avian-like PB2-627E and human-like PB2-627K, overcoming host restrictions and posing a risk for human pandemics. Specifically, by screening the global PB2 sequences, we discovered a new independent cluster with PB2-627V emerged in the 2010s, which is prevalent in various avian, mammalian, and human isolates of AIVs, including H9N2, H7N9, H3N8, 2.3.4.4b H5N1, and other subtypes. And, the increasing prevalence of PB2-627V in poultry is accompanied by a rise in human infection cases with this variant. Then we systematically assessed its host adaptation, fitness, and transmissibility across three subtypes of AIVs (H9N2, H7N9, and H3N8) in different host models, including avian and human cells, chickens, mice, and ferrets where infections naturally occur. We found that PB2-627V facilitates AIVs to efficiently infect and replicate in chickens and mice by utilizing both avian- and human-origin ANP32A proteins. Importantly, and like PB2-627K, PB2-627V promotes efficient transmission between ferrets through respiratory droplets. Deep sequencing in passaged chicken samples and transmitted ferret samples indicates that PB2-627V remains stable across the two distinct hosts and has a high potential for long-term prevalence in avian species. Therefore, the mutation has the ability to continue spreading among poultry and can also overcome the barrier between birds and humans, greatly enhancing the likelihood of AIVs infecting humans. Given the escalating global spread of AIVs, it is crucial to closely monitor influenza viruses carrying PB2-627V to prevent a pandemic.

Introduction

Avian influenza viruses (AIVs) are critically important in the evolution of pandemic influenza viruses [1]. Adaptive changes in AIVs allow breakthrough infection in mammalian species through altering viral interactions with host-specific factors [2–4]. The current clade 2.3.4.4b highly pathogenic avian influenza (HPAI) H5Ny virus outbreaks have swept across continents, posing an unprecedented panzootic threat to birds, mammals, and public health [5] (https://www.who.int/news/item/12-07-2023-ongoing-avian-influenza-outbreaks-in-animals-pose-risk-to-humans). Other subtypes of AIVs have also been responsible for recurrent human infections [6]. For example, H7N7 [7], H7N9 [8,9], H10N8 [10], H5N6 [11], H10N3 [12] and H3N8 [13] viruses have caused over 1600 documented human cases [11]. Notably, most of these AIV subtypes possess internal (i.e. non-glycoprotein) genes that are derived from avian H9N2 viruses [8,11–13]. H9N2 virus is globally widespread in wild and domestic birds [14,15], and causes repeated human infections, especially since 2015. In these interspecies transmission events, critical adaptive mutations often occur on the PB2 protein of AIVs [12,16–19].

PB2 is one of three polymerase subunits of the influenza virus RNA-dependent RNA polymerase (RdRP), crucial for genome transcription and replication [20]. Specific amino acid changes have been identified in PB2 as key determinants of avian-to-mammalian adaptation, through its interaction with host acidic leucine-rich nuclear phosphoprotein 32 (ANP32) in avian and mammalian cells [21–24]. Their interactions exhibit host-species specificity [23]. PB2-627K in human influenza viruses interacts with human ANP32A and ANP32B (huANP32A and huANP32B) to support viral polymerase function [22]. On the other hand, PB2-627E in AIV can utilize avian ANP32A, but not huANP32A or huANP32B [22]. PB2-E627K amino acid substitution in AIVs promotes viral polymerase activity in mammalian cells by enhancing PB2

67 interaction with huANP32A and huANP32B [25]. Fortunately, the PB2-627K genotype is only
68 frequently detected in AIVs isolated from human infections, and rarely detected in AIVs isolated
69 from poultry or wild birds [26], greatly reducing the possibility of AIVs transmission to humans.
70 In this study, we discovered an emerging PB2-627 polymorphism (PB2-627V) in diversified
71 subtypes that increases the pandemic potential of AIVs by breaking through ANP32 host
72 restriction in mammalian and avian hosts.

73 # Results

74 ## PB2-627V prevalence in influenza virus isolates from avian and
75 ## mammalian species

76 Given the crucial role of PB2 residue 627 in host adaptation, we analyzed 42,297 influenza
77 PB2 sequences worldwide (excluding human H3N2 and H1N1pdm09 viruses) for polymorphisms
78 at this position. We found that the number of sequences with PB2-627V rapidly increased after
79 2016 (Fig 1A). Among these viruses with PB2-627V, 71.3% were isolated from avian species,
80 14.7% were from humans, 14.0% were from other mammalian hosts (such as fox, swine, tiger, and
81 mink) and environment (Fig 1A and S1 Table). In geographical distribution, 61.7% of the viruses
82 were isolated in China, with the remaining (38.3%) found in the Middle East, Germany, Mexico,
83 Canada, Italy, Spain, Russia, America, Denmark, and Belgium (Fig. 1A, and S1 Table). In terms
84 of subtype distribution, 64.5% of PB2-627V variants were detected in H9N2 viruses, 9.9% in
85 H7N9 and 9.1% in H5N6 viruses; the remaining 16.5% were in various other subtypes: H1N1,
86 H1N2, H3N2, H3N8, H5N1, H5N2, H6N6, H7N1, and H10N3 (Fig. 1A, and S1 Table). Notably,
87 PB2-627V has also been identified in clade 2.3.4.4b H5N1 viruses isolated from wild birds and
88 red foxes (Fig. 1A, and S1 Table).

89 In phylogenetic analysis, recent PB2-627V sequences mainly belong to a major group that
90 includes most human and avian isolates from multiple subtypes (H9N2, H7N9, H5N6, H3N8,
91 H10N3, and H5N1 viruses) (Fig 1B). For H9N2 subtype, PB2 gene showed the evolution of a
92 PB2-627V cluster (S1A Fig). Ancestral host reconstruction on time-scaled phylogeny indicated
93 that chicken isolates are the origin of human isolates within this cluster (S1B Fig). Notably, PB2-
94 627V of H9N2 is more frequently detected in humans than avian isolates from 2016-2022 (Fig
95 1C). Similarly, there was a dramatic increase in PB2-627V detection in avian and human hosts for
96 the H7N9, H5N6, and H3N8 subtypes after 2016 (S2 Fig). Thus, it appears that PB2-627V has
97 achieved better adaptability in poultry populations and its emerging prevalence both in avian and
98 humans suggests functional significance across various host species.

99 PB2-627V promotes polymerase activity of H9N2 AIV in human and 100 chicken cells by utilizing ANP32 proteins of both host species

101 To evaluate the functionality of PB2-627V, we used a previously identified chicken H9N2
102 isolate A/chicken/Hubei-m0530/2017 (referred to as 17/H9N2^{627E}) with PB2-627E as the
103 backbone, and introduced the PB2-E627V and PB2-E627K changes. Although PB2-627V and -
104 627K are found in other natural chicken isolates, this approach allowed the dissection of the
105 function of this single mutation. A dual-luciferase assay system was used to compare viral
106 polymerase activities conferred by PB2-627E, V, and K in avian DF-1 cells and human 293T cells
107 at 33°C and 37°C, respectively, mimicking the temperature of human upper and lower respiratory
108 tract [27]. In DF-1 cells, 17/H9N2^{627E}, 17/H9N2^{627V}, and 17/H9N2^{627K} showed comparable
109 polymerase levels at 33°C and 37°C (Fig 1D). However, a 23.6-fold (±2.6) increase in polymerase
110 activity at 33°C, and an 11.8-fold (±0.6) increase at 37°C were found with 17/H9N2^{627V} in 293T

111 cells compared with 17/H9N2^{627E} ($p < 0.001$); 17/H9N2^{627K} exhibited a 9.3-fold (±2.6) increase in
112 polymerase activity at 33°C and a 20.2-fold (±0.4) increase at 37°C ($p < 0.001$) relative to
113 17/H9N2^{627E} (Fig. 1E). Accordingly, in avian DF1 cells, PB2-627V demonstrated more robust
114 viral transcriptional and replication functions than PB2-627K, while in human A549 cells, it
115 surpassed PB2-627E (S3A and S3B Fig).

116 Viral polymerase activity was further examined in ANP32A and ANP32B double-knockout
117 293T (DKO) cells over-expressing chicken- or human-ANP32 protein(s) [25]. As expected,
118 polymerase activities of all 3 viruses (17/H9N2^{627E}, 17/H9N2^{627V}, and 17/H9N2^{627K}) in control
119 DKO cells were significantly lower than those in the wild type 293T cells (S3C Fig). Polymerase
120 activity of 17/H9N2^{627E} in the DKO cells was significantly enhanced in the presence of chicken
121 ANP32A (chANP32A) at both 33°C and 37°C ($p < 0.05$) (Fig 1F). With 17/H9N2^{627V}, chANP32A
122 in DKO cells significantly enhanced the polymerase activity at both 33°C and 37°C ($p < 0.05$),
123 and huANP32A significantly enhanced polymerase activity only at 37°C ($p < 0.001$) (Fig 1F).
124 With 17/H9N2^{627K}, expression of chANP32A in DKO cells significantly enhanced viral
125 polymerase activity only at 37°C ($p < 0.001$), and huANP32A and huANP32B significantly
126 enhanced the polymerase activity at both 33°C and 37°C ($p < 0.001$) (Fig 1F).

127 ANP32 interface with PB2 at the 627-domain by electrostatic and hydrophobic interactions
128 [28]. PB2-627K (lysine) has a positive charge and PB2-627E (glutamic acid) has a negative charge.
129 Modeling the surface electrostatic potential predicted that valine at PB2-627 confers a neutral state
130 (Fig 1G), which could permit the PB2 protein to interact sufficiently with avian and human
131 ANP32A proteins to promote viral polymerase activity in avian and human cells. In summary,
132 these findings indicate that PB2-627V can utilize chicken and human ANP32A in the respective
133 species of cells to facilitate viral polymerase activity.

PB2-627V in H9N2 virus maintains efficient replication in chickens and facilitates replication in human cells and mice

Next, viruses with the three PB2 627 polymorphisms were rescued on the background of the 17/H9N2 virus. The replication kinetics of these 17/H9N2^{627E}, 17/H9N2^{627V}, and 17/H9N2^{627K} viruses were assessed in avian CEF cells; no significant differences in replication were found between viruses ($p > 0.05$) (Fig 2A). Chickens individually inoculated with 10^6 EID_{50} of each virus showed no mortality (S4A Fig) and no apparent clinical signs. Viral loads detected from oropharyngeal swabs of 17/H9N2^{627V} and 17/H9N2^{627E} inoculated chickens were significantly higher than those infected with 17/H9N2^{627K} at 6 and/or 8 dpi ($p < 0.05$) (Fig 2B). The three viruses replicated to comparable titers in the turbinates at 3 dpi, but 17/H9N2^{627V} replicated to higher titers than 17/H9N2^{627K} in the lungs ($p < 0.05$) (Fig 2C). Histopathological examination of chicken lungs at 3 dpi indicate that all viruses induced inflammatory responses, with more hemorrhage noted in 17/H9N2^{627V} infected lungs (Fig 2D). These findings indicate that PB2-627V and PB2-627E replicated comparably well in chickens.

In infected human A549 cells, virus titers of 17/H9N2^{627V} and 17/H9N2^{627K} were significantly higher than that of 17/H9N2^{627E} from 12 to 48 hpi ($p < 0.001$); there was no significant difference between 17/H9N2^{627V} and 17/H9N2^{627K} ($p > 0.05$) (Fig 2E). Mice inoculated with 17/H9N2^{627E}, 17/H9N2^{627V}, or 17/H9N2^{627K} virus, showed no obvious clinical signs, as in infected chickens (Fig 2F and S4B Fig). Higher virus loads were detected in the nasal turbinates and lungs of mice infected with 17/H9N2^{627V} and 17/H9N2^{627K} at 3 dpi than those with 17/H9N2^{627E} ($p < 0.001$); there was no significant difference in virus titers between the 17/H9N2^{627V} and 17/H9N2^{627K} groups ($p > 0.05$) (Fig 2G). Likewise, 17/H9N2^{627V} and 17/H9N2^{627K} viruses produced more viral

156 NP protein-positive cells in the lung than in corresponding 17/H9N2^{627E} infected mice (Fig 2H).
157 Thus, the infectivity of PB2-627V H9N2 virus in human cells and mice is similar to that of PB2-
158 627K virus.

159 PB2-627V confers aerosol transmission of H9N2 virus in ferrets

160 Transmissibility of influenza viruses between ferrets is an indicator of potential epidemic or
161 pandemic risk. Direct contact (DC) and respiratory droplet (RD) transmission tests of the
162 17/H9N2^{627E}, 17/H9N2^{627V}, and 17/H9N2^{627K} viruses were performed in ferrets. All viruses
163 infected the directly infected donor animals, as assessed by virus titers in nasal washes (Fig. 3A-
164 3C, and S2 Table). 17/H9N2^{627V} and 17/H9N2^{627K} viruses were transmitted to all DC ferrets and
165 all RD ferrets, but 17/H9N2^{627E} was only transmitted to DC groups. Transmission by RD in the
166 17/H9N2^{627V} group took place around 2 days later than in the 17/H9N2^{627K} group (Fig 3A-3C).
167 Areas under the curve (AUC), based on virus titers over time in the nasal washes, were determined
168 to compare total viral shedding during infection (Fig 3D and S3 Table). In donor ferrets, virus
169 production was comparable between the three viruses. In DC ferrets, 17/H9N2^{627V} virus output
170 (AUC = 18.13 ± 3.69) was slightly higher than that of 17/H9N2^{627E} virus (14.13 ± 3.01, $p = 0.19$)
171 and 17/H9N2^{627K} virus (16.25 ± 1.27, $p = 0.68$). In RD ferrets, 17/H9N2^{627V} virus output (AUC =
172 11.75 ± 2.88) was slightly lower than that of 17/H9N2^{627K} virus (15.42 ± 1.60, $p = 0.25$) (Fig 3D
173 and S3 Table). Thus, in contrast to PB2-627E, PB2-627V promotes aerosol transmissibility of
174 H9N2 virus in ferrets.

175 To monitor any polymorphic changes at residue PB2-627 during virus infection and
176 transmission, next-generation sequencing was performed on nasal wash samples from each ferret
177 at the first and the last time points of positive virus detection. In 17/H9N2^{627E} groups, 627E
178 remained the dominant genotype in the donors and DC ferrets (Fig 3E). In the donor groups of

179 17/H9N2^{627V} and 17/H9N2^{627K}, 627V and 627K were the corresponding dominant genotypes. In
180 the DC and RD transmission groups of 17/H9N2^{627V} and 17/H9N2^{627K}, polymorphisms at PB2-
181 627 during infection were more noticeable, but at the last detection time point of each RD group,
182 corresponding 627V and 627K returned to their earlier dominance (Fig 3F and 3G). These results
183 suggest that residue PB2-627V stably confers aerosol transmission of H9N2 virus in ferrets.

184 PB2-627V has the potential for sustained prevalence in poultry

185 17/H9N2^{627E}, 17/H9N2^{627V}, and 17/H9N2^{627K} H9N2 viruses were serially passaged in
186 chickens to assess the potential for sustained prevalence of PB2-627V in poultry. Chickens were
187 directly infected with each virus (Passage 1, P1) and subsequently (P2 - P5) passaged through
188 contact transmission (Fig 4A). All viruses were successfully passaged from P1 to P5. We then
189 performed next-generation sequencing of whole viral genomes from RNA isolated from the lungs
190 of the P5 chickens. Mutations above 1% threshold were identified as intra-host single nucleotide
191 variants (iSNVs) [29,30]. Overall, most iSNVs were detected at low frequency and there were no
192 significant differences between the 3 groups (Fig 4B). Notably, variant frequency at residue PB2-
193 627 was below the 1% threshold in all P5 chicken samples (Fig 4C). At the amino-acid level, two
194 variant residues (PA-D529N, NP-T211D) occurred at a high frequency (>10%) in the 17/H9N2^{627K}
195 group, but no high-frequency variant residues were detected in 17/H9N2^{627E} and 17/H9N2^{627V}
196 groups (Fig 4D), suggesting that compared to PB2-627E and PB2-627V, PB2-627K required other
197 cooperative mutations in RNP genes for transmission in chickens. Taken together, PB2-627V
198 showed a high potential for sustained prevalence in chickens.

199 **PB2-627V confers dual ability to replicate in chickens and mice to**

200 **avian H7N9 and H3N8 viruses**

201 We determined if the dual host adaptability of PB2-627V, detected at high frequency in the
202 H9N2 virus, is transferrable to other AIV subtypes. H7N9 and H3N8 viruses possess the PB2 gene
203 and other internal genes derived from the H9N2 viruses [9,31]. The natural mutations PB2-E627V
204 and PB2-E627K were separately introduced into the LPAI H7N9 (A/chicken/China/0606-12/2017,
205 referred as 17/H7N9^{627E}) and H3N8 (A/chicken/Anhui/FE12/2022, referred as 22/H3N8^{627E}) [32]
206 viruses. The resulting PB2-627V, PB2-627K, and PB2-627E viruses were assessed for replication
207 and pathogenicity in chickens and mice.

208 In chickens, introduction of PB2-E627V or PB2-E627K mutation into 17/H7N9 and 22/H3N8
209 viruses did not significantly affect replication or pathogenicity relative to their PB2-627E
210 counterparts (Fig 5A-5E), although the replication of 17/H7N9^{627V} in chicken lungs was
211 significantly higher than that of 17/H7N9^{627K} ($p<0.05$) (Fig 5B). Thus, PB2-E627V had little effect
212 on virus replication and pathogenicity in chickens (Fig. 5A-5E, and S5A Fig). In mice, both PB2-
213 E627V and PB2-E627K changes in 17/H7N9 and 22/H3N8 viruses led to virus loads in the nasal
214 turbinates and lungs, weight loss, and mortality ($p<0.01$) (Fig 5F-5K). Murine lungs at 3 dpi. with
215 subtypes housing PB2-627V showed more severe pathology than those with PB2-627E (Fig 5L
216 for 17/H7N9 and S5B Fig for 22/H3N8). In summary, PB2-E627V significantly increases
217 pathology and replication of H7N9 and H3N8 virus subtypes in mice and maintains their
218 replication fitness in chickens.

219 # Discussion

220 Here, we identified PB2-627V as an emerging variant in AIVs with significant zoonotic and
221 pandemic potential. We observed that PB2-627V enhances the polymerase activity of H9N2 AIV
222 in both human and chicken cells by utilizing ANP32A proteins from both species, thereby
223 overcoming the restriction imposed by human ANP32 on AIVs carrying PB2-627E and exhibiting
224 properties similar to those with PB2-627K. PB2-627V in H9N2 virus maintains efficient
225 replication in chickens, facilitates virus replication in mice, and confers aerosol transmission in
226 ferrets. Furthermore, PB2-627V is stably maintained in passages through chickens and also
227 conferred the dual ability to replicate in chickens and mice to avian H7N9 and H3N8 subtype
228 viruses. Thus, the increased prevalence of this dual adaptive mutation of PB2-E627V in poultry
229 greatly increases the chances of AIVs infecting humans. In addition, the wide distribution of this
230 mutation in multiple subtypes, hosts, and countries poses global public health risks.

231 Clinical data and phylogenetic analysis revealed that residue PB2-627V originated in chicken
232 influenza viruses (likely the H9N2 subtype) and was subsequently transmitted to humans. The
233 prevalence of PB2-627V in AIVs is on the rise, particularly within the H9N2 subtype, and PB2-
234 627V is also found in other subtypes such as H7N9, H5N6, H3N8, and H10N3, which contain
235 reassorted internal genes derived from H9N2 [8,11–13]. Serial passage studies in chickens further
236 indicate that additional mutations occurred in the polymerase protein after the passage of H9N2
237 viruses with the PB2-E627K. However, H9N2 viruses with PB2-627E and -627V did not produce
238 further mutations. This may be due to the PB2-627K mutation still having defects in transmission
239 in chickens and requiring further adaptation. This could explain why PB2-627K is very rare in
240 avian isolates. The PB2-E627K mutation usually takes place in infected humans [33]. Conversely,
241 PB2-627V appears to be a product of evolution in H9N2 virus and has a high potential for long-

242 term prevalence in poultry populations, posing an increasing likelihood of viral transmission to
243 humans.

244 Cellular ANP32 proteins specifically support influenza virus genome replication. ANP32A
245 can bridge PB2 dimers and form extensive contacts with two polymerases to maintain a dimeric
246 assembly [22,34]. The C-terminal low complexity acidic region (ANP32A^{LCAR}) inserts between
247 two PB2-627 domains of the polymerase dimer. Human ANP32A^{LCAR} contains only acidic amino
248 acid residues. Thus, with human ANP32A, basic or uncharged residues (such as lysine, K or valine,
249 V) are preferred in the PB2-627 domain to acidic amino acids (such as glutamic acid, E) [21,22].
250 In avian cells, the additional 33 amino acids in chANP32A^{LCAR} allow AIVs carrying PB2-627E to
251 effectively utilize chANP32A in avian cells [23,35]. Indeed, in the context of H9N2, we found that
252 the polymerase activity of PB2-627V in avian cells is comparable to PB2-627E, and in human
253 cells is comparable to PB2-627K which suggests that the nonpolar neutral amino acid of PB2-
254 627V has the dual ability to interact with avian ANP32A and human ANP32A in different host
255 cells. It is noteworthy that, when the PB2-627 site is changed from E to V, the virus can not only
256 undergo contact transmission in ferrets but also undertake effective aerosol transmission, similar
257 to that of the 17/H9N2^{627K} variant. In addition, PB2-627V can be maintained in ferret post-
258 infection, during contact and aerosol transmission. Thus, these features suggest that the dual
259 adaptive PB2-627V AIVs reduce the host barrier between avians and humans.

260 The PB2-E627V has been identified in H5N1 viruses where it was shown to increase viral
261 replication in mammalian cells and virulence in mice [36], while in the background of a laboratory
262 strain of H1N1 (PR8), it reduced viral replication in mammalian cells compared with PB2-627K
263 [37]. However, because the PB2-627V variant was rarely found in natural influenza isolates at that
264 time (before 2015), it did not attract much attention. In H9N2 AIVs, PB2-627V variants appeared

265 in the Middle East from 2000 to 2015 but were not stably maintained. The genotype of Middle
266 East H9N2 viruses was very different from the G57 lineage [8] H9N2 virus prevalent in China and
267 studied here [38,39]. Under experimental conditions, PB2-627V in the Middle East H9N2 virus
268 needs to operate in concert with PB2-E543D, PB2-A655V and PB2-K526R to enhance viral
269 replication in mammals [38]. Numerous adaptive mutations have recently been identified in the
270 G57 H9N2 virus, including PB2-292, PB2-588, PA-356, M1-37 and HA-226 [15,40,41], in avian
271 and human isolates [42–45]. It is plausible that one or more of these adaptive changes in the G57
272 genotype exert epistatic effects to induce the emergence of the stable PB2-627V residue, but this
273 remains to be tested.

274 Collectively, our results suggest that the recent evolved variant PB2-E627V combines the
275 characteristics of avian-like PB2-627E and human-like PB2-627K. It exhibits a crucial dual-
276 adaptation that can effectively infect and transmit in both avian and mammalian hosts, thereby
277 overcoming the interspecific barrier between birds and humans. The presence of PB2-627V in
278 multiple subtypes of AIVs undoubtedly escalates the risk of an avian influenza virus pandemic.
279 We therefore recommend considering PB2-627V as a new molecular marker to assess the
280 pandemic potential of AIVs.

281 Materials and Methods

282 Ethics statement

283 9 to 11-day-old specific pathogen-free (SPF) embryonated chicken eggs and all experimental
284 animals were purchased from Boehringer Ingelheim, China. All animal research was approved by
285 the Beijing Association for Science and Technology (approval ID SYXK, Beijing, 2020-0053) and
286 performed in compliance with the Beijing Laboratory Animal Welfare and Ethics guidelines, as

287 issued by the Beijing Administration Committee of Laboratory Animals, and by the China
288 Agricultural University (CAU) Institutional Animal Care and Use Committee guidelines (ID:
289 SKLAB-B-2010-003) approved by the Animal Welfare Committee of CAU. The H9N2, H7N9,
290 and H3N8 wild-type viruses used are all low pathogenic avian influenza (LPAI) viruses isolated
291 from chickens. PB2-E627V and PB2-E627K are natural mutations found in these viruses.

292 Sequence collection and alignment

293 The sequences of the PB2 gene were obtained from the GISAID database
294 (http://www.gisaid.org). After removing the PB2 sequences of human H3N2 and H1N1pdm09
295 viruses and duplicate sequences, a total of 42,297 full-length PB2 sequences of IAVs published
296 globally from 1994 to 2022 were obtained. All accession codes of public sequences can be found
297 in Dataset S1. Sequences were aligned using MUSCLE v3.7 [46] via the CIPRES Science Gateway
298 [47].

299 Phylogenetic analyses

300 The phylogenetic tree of the H9N2 PB2 gene was constructed using a total of 4523 PB2
301 sequences from H9N2 subtype IAVs. The phylogenetic tree of PB2-627V was constructed using
302 a total of 394 PB2 sequences carrying the PB2-627V. IQ-TREE version 1.6 was used to construct
303 the maximum likelihood phylogenetic trees, applying the best-fit general time-reversible model of
304 nucleotide substitution with gamma-distributed rate variation among sites (GTR + I + G), and
305 performing ultrafast bootstrap resampling analysis (1000 replications). Phylogenetic trees were
306 visualized and annotated using FigTree version 1.4.4, Adobe Illustrator 2021, and Interactive Tree
307 Of Life (iTOL) [48].

308 ## Host transmission dynamics analyses

309 A maximum clade credibility (MCC) tree was performed on the PB2-627V cluster sequences
310 (Fig. S1A) with BEAST v1.10.4. Using the coalescent Bayesian Skygrid model, the General Time
311 Reversible (GTR) model of evolution and the strict clock were employed. The host jump patterns
312 were interfered by mapping the host types onto the time-scaled tree using an asymmetric discrete
313 trait model [49]. A Markov Monte Carlo (MCMC) chain is run for 30 million, sampled every 3000
314 and the first 10% of tree was removed as burn-in. Stationarity and mixing were checked with
315 Tracer v1.7.2. The MCC tree was finally generated by TreeAnnotator and visualized using FigTree
316 v1.4.4.

317 ## PB2 protein structure simulation

318 A simulation of the A/chicken/Hebei/m0530-1/2017 (17/H9N2) PB2 protein structure was
319 performed by using Swiss-Model (https://swissmodel.expasy.org). The 17/H9N2 PB2 protein
320 sequence was inputted in FASTA format, and the published H7N9 protein structure (PDB: 7qtl.1.C)
321 with 98.94% sequence identity was utilized as the template. The quality of the resulting model was
322 evaluated using GMQE and QMEAN scores. PyMOL was utilized to introduce the PB2-E627V
323 and PB2-E627K mutations into the model and to ascertain the surface charge of the protein.

324 ## Cell lines

325 Human lung epithelial cell (A549) cells, kidney epithelial (293T) cells, chicken fibroblast
326 (DF-1) cells, and Madin-Darby Canine Kidney (MDCK) cells were maintained in our laboratory.
327 Chick embryo fibroblast (CEF) cells were obtained from SPF embryonated chicken eggs as
328 previously described [50]. 293T cell line with a double knockout of ANP32A and ANP32B (DKO
329 cell) was kindly provided by Xiaojun Wang from Harbin Veterinary Research Institute. Cells were

330 cultured with Dulbecco's modified Eagle medium (DMEM; Gibco, New York, USA)
331 supplemented with 10% fetal bovine serum (FBS; Gibco, Sydney, Australia) and 1% penicillin-
332 streptomycin solution (MACGENE, Beijing, China).

333 Influenza viruses

334 H9N2 AIV A/chicken/Hebei/m0530-1/2017 (17/H9N2) was characterized and maintained in
335 our laboratory. Influenza H7N9 virus A/chicken/China/0606-12/2017 (17/H7N9) and influenza
336 H3N8 virus A/chicken/Shandong/FE12/2022(H3N8) (22/H3N8) were isolated by our laboratory.
337 Viruses were propagated in 9 to 11-day-old SPF embryonated chicken eggs at 35°C for 72 hours.
338 Virus titers were determined by 50% tissue culture infectious dose ($TCID_{50}$) on MDCK cells or
339 50% egg infectious dose (EID_{50}) on SPF chicken eggs.

340 Animals

341 5 to 6 weeks-old female SPF BALB/c mice and 6 to 8 weeks-old female SPF chickens were
342 purchased from Vital River Laboratory Animal Technology Co., Ltd (Beijing, China). Mice were
343 kept in individually ventilated cages (IVC), and chickens were kept in high efficiency particulate
344 air (HEPA)-filter isolators in the Animal Care Facilities at CAU. Five to six-month-old male
345 Angora ferrets (*Mustela putorius furo*), serologically negative for currently circulating influenza
346 viruses (H1, H3, H5, H7, and H9) and > 1.0 kg (ranging from 1.10 to 1.80 kg) in weight, were
347 purchased from Angora LTD (Jiangsu, China). All ferrets were housed in wire cages placed inside
348 HEPA-filter isolators. All animals were allowed free access to water and a standard chow diet, and
349 provided with a 12-hour light and dark cycle (temperature: 20-25°C, humidity: 40%-70%). All
350 animals used were not involved in any other experimental procedure.

351 ## Generation of viruses by reverse genetics

352 As described previously [18], recombinant viruses were generated using a plasmid-based
353 reverse genetics system in the genetic background of 17/H9N2, 17/H7N9, and 22/H3N8.
354 Mutations were introduced into the plasmids using PCR-based site-directed mutagenesis. To check
355 for the absence of unintended mutations, all propagated viruses were subjected to complete
356 sequencing.

357 ## Polymerase activity assay

358 To compare the polymerase activities of different viral ribonucleoprotein (RNP) complexes,
359 a dual-luciferase reporter assay system (Promega, Madison, WI, USA) was employed [25]. The
360 PB2, PB1, PA, and NP gene segments of respective viruses were individually cloned into the
361 pCDNA3.1 expression plasmid. 125 ng of each of the PB2, PB1, PA, and NP plasmids, as well as
362 10 ng of the pLuci luciferase reporter plasmid and 2.5 ng of the Raniera internal control plasmid,
363 were transfected into 293T cells or DF-1 cells. The cell cultures were then incubated at 33°C or
364 37°C for 24 hours. The transfected cells were then lysed and analyzed for firefly and renilla
365 luciferase activities using a GloMax 96 microplate luminometer (Promega). The function of
366 ANP32 was examined using a polymerase assay by co-transfection of DKO cells with different
367 ANP32 proteins or empty vector (20 ng) at 33°C or 37°C for 24 hours. All of the experiments were
368 performed independently at least three times.

369 ## Growth kinetics of viruses in A549 and CEF cells

370 A549 and CEF cells were cultured in 6-well plates and infected in triplicate with indicated
371 viruses at a multiplicity of infection (MOI) of 0.1 (A549) or 0.01 (CEF). After a 2-hour incubation,
372 cells were washed three times with DPBS, and incubated at 37°C in 5% CO_2. Supernatants were

373 collected at 12, 24, 36, 48, and 60 hours post-infection (hpi), and virus titers were determined by
374 $TCID_{50}$ assays on MDCK cells.

375 Quantitative real-time PCR assay

376 Levels of mRNA and viral RNA (vRNA) were determined in A549 cells and DF-1 cells
377 infected in triplicate with viruses (17/H9N2^{627E}, 17/H9N2^{627V}, or 17/H9N2^{627K}) at an MOI of
378 0.1(A549 cells) or MOI of 0.001 (DF-1 cells). Total RNA was extracted from infected cells by
379 using TRIzol reagent according to the manufacturer's instructions (Invitrogen). For the detection
380 of mRNA and vRNA, the oligo(dT) primer and primer uni-12 (5'- AGCAAAAGCAGG -3') were
381 used respectively to generate cDNAs from 1 μg of total RNA per sample by using Superscript III
382 first-strand synthesis supermix (Invitrogen). The quantitative real-time PCR (qRT-PCR) mixture
383 for each reaction sample consisted of 10 μL of 2× SYBR green PCR master mix (Applied
384 Biosystems), 7 μL of nuclease-free water, 0.5 μL of each primer, and 2 μL of the cDNA template.
385 qPCR was conducted using a 7500 real-time PCR system (Applied Biosystems) with the following
386 program: 1 cycle at 95°C for 10 min, followed by 40 cycles of 95°C for 15 s and 60°C for 1 min.
387 Expression values for each gene, relative to *β-actin*, were calculated by using the $2^{-\Delta\Delta CT}$ method.
388 Each qPCR sample contained three technical replicates. Primers for the amplification of the *β-*
389 *actin* and PB2 genes are as follows: forward primer 5'-AGAGCTACGAGCTGCCTGAC-3' and
390 reverse primer 5'-CGTGGATGCCACAGGACT-3' for *β-actin*, forward primer 5'-
391 GGAACAGGAATGGACCGACA-3' and reverse primer 5'-ACTGAGATCTGCATGACCCG-3'
392 for PB2.

393 ## Mouse challenge studies

394 Groups of eight mice were anesthetized by intramuscular injection of Zoletil 50 (Zoletil;
395 Virbac SA, Carros, France) at a dose of 20 mg/kg, and inoculated intranasally (i.n.) with 10^6
396 $TCID_{50}$ of test virus or PBS in a total volume of 50 μL. At 3 days post-infection (dpi), 3 mice from
397 each group were euthanized, and lung and nasal turbinate tissues were collected for virus titration
398 in MDCK cells by $TCID_{50}$ assay. Lungs of mice infected with the indicated viruses at 3 dpi were
399 collected for histopathology and immunohistochemistry (IHC). The remaining 5 animals were
400 monitored in the remaining two weeks for disease progression, weight change, and mortality. Mice
401 that experienced a weight loss exceeding 25% of their original weight were humanely euthanized.

402 ## Chicken challenge studies

403 Experimental procedures for virus infection of chickens were under previously described
404 protocol [51]. Groups of 6 chickens were inoculated i.n. with 10^6 EID_{50} of indicated virus or PBS
405 in a volume of 200 μL. At 3 dpi, 3 chickens from each group were euthanized, and lung and nasal
406 turbinate tissues were collected for virus titration by EID_{50} assay. Lungs of chickens at 3 dpi were
407 collected for histopathology and IHC. The remaining 3 chickens were monitored and tracheal
408 swabs were taken at 2, 4, 6, and 8 dpi for virus titration by EID_{50} assay.

409 ## Histopathology and IHC analysis

410 Lungs were fixed in 10% buffered formalin, embedded in paraffin, sectioned and stained with
411 hematoxylin and eosin (H&E). Tissue sections were also immunostained with a viral NP
412 monoclonal primary antibody (ab20343, Abcam, Beijing, China). The secondary antibody used
413 was conjugated to horse radish peroxidase (HRP), and the color reaction was based on the use of

414 an HRP reaction kit (ZSGB-BIO, Beijing, China). Histopathological examination was conducted
415 blind by two experienced experimental pathologists.

416 Virus passage in chickens

417 For virus passage in chickens, as depicted in Fig. 4A, groups of 2 SPF chickens were
418 inoculated at passage 1 (P1) with 10^6 EID_{50} of the indicated virus in a volume of 200 μL. At 3 dpi,
419 2 naïve chickens were co-housed with the P1 chickens to establish the P2 generation. At 6 dpi of
420 P1 chickens, lung tissues of P1 chickens were collected and homogenized in 500 μL of cold PBS,
421 and another 2 naïve chickens were introduced as P3. The same sequential steps were used for
422 passage up to the P5.

423 Ferret transmission experiments

424 The transmission study consisted of groups of 3 ferrets, following a previously described
425 protocol[32,52] comprising one infected, one direct contact (DC), and one respiratory droplet
426 contact (RD) group. Ferrets were housed in wire cages inside isolators, with each isolator
427 approximately 15 cubic feet in size. Each ferret was sedated with ketamine (20 mg/kg) and
428 xylazine (1 mg/kg) via intramuscular injection and inoculated intranasally with 10^6 $TCID_{50}$ of
429 17/H9N2^{627E}, 17/H9N2^{627V}, or 17/H9N2^{627K} virus in a volume of 500 μL delivered at 250 μL per
430 nostril. Twenty-four hours later, 2 naïve ferrets were introduced into the isolator, with the direct
431 contact ferret placed in the same cage as the infected ferret, while the respiratory droplet contact
432 ferret was placed in a cage separated by a wire mesh wall to prevent physical contact.

433 Individual weight was monitored throughout the study. Nasal washes were collected from the
434 ferrets by 2 mL virus transport medium every other day for 14 days and titrated for viruses in
435 MDCK cells by TCID50 assays. Additionally, 200 μL nasal washes were used for RNA extraction

436 and deep sequencing. At 21 dpi, blood samples of ferrets were collected to determine
437 seroconversion using the HI Assay.

438 Next generation sequencing

439 A total of 54 ferret nasal wash samples, 6 chicken lung samples, and 3 viruses (17/H9N2^{627E},
440 17/H9N2^{627V}, and 17/H9N2^{627K}) were subjected to whole-genome sequencing. Viral RNA was
441 harvested from the samples by using the QIAamp Viral RNA Mini Kit (Qiagen). Multiplex reverse
442 transcription-PCR amplification of all 8 influenza virus genome segments was performed on RNA
443 samples using PrimeScript™ II 1st Strand cDNA Synthesis Kit (Takara 6210) and primers
444 Uni12/Inf1 (5'-GGGGGGAGCAAAAGCAGG-3'), Uni12/Inf3 (5'-
445 GGGGGAGCGAAAGCAGG-3'), and Uni13/Inf1 (5'CGGGTTATTAGTAGAAACAAGG-3').
446 As previously described [32], PCR products were purified on spin columns and quantified by using
447 the Quant-It Pico Green kit (Invitrogen, Carlsbad, USA). The purified amplicons were pooled in
448 equimolar and paired-end sequenced (23150) on an Illumina NovaSeq platform according to the
449 standard protocols. Sequencers by 200 or 250 bp paired-end sequencing, and sequencing depth for
450 avian influenza virus isolates was about 0.2 G per sample. NGS findings were validated by qRT-
451 PCR. Raw NGS reads were processed by filtering out low-quality reads (eight bases with quality
452 < 66), adapter-contaminated reads (with > 15 bp matched to the adapter sequence), poly-Ns (with
453 8 Ns), duplication and host-contaminated reads (SOAP2 [version 2.21]; less than five mismatches).
454 Sanger sequences of parental viruses were chosen as reference sequences. Burrows-Wheeler
455 Alignment Tool (version 0.7.12) and SAMtools (version 1.4) were then used to perform reference-
456 based assembly. Data analyses were performed using a custom quality-based variant detection
457 pipeline.

To detect the genomic variants, the iSNVs were identified as following standards: 1) reads > 1000; 2) mutation rates >1%. The iSNVs frequency was calculated by using the number of iSNVs divided by the total number of genome sites.

Quantification and statistical analysis

Graphing and statistical analyses were performed using GraphPad Prism 8 (GraphPad Software, San Diego, California, USA; www.graphpad.com). Experimental groups were statistically compared by analysis of variance (ANOVA). P value < 0.05 was considered to indicate statistical significance.

Acknowledgments

We thank the Global Initiative on Sharing Avian Influenza Data (GISAID) for sharing the influenza virus sequence data used in this study. We are grateful to Xiaojun Wang (Harbin Veterinary Research Institute, China) for providing the DKO cells, Shangang Jia (China Agricultural University, China) for helpful suggestions on data analysis, and Nianzhi Zhang (China Agricultural University, China) for constructive suggestions on structure analysis. We thank BioRender (biorender.com) for assisting with graphics.

Funding

National Key Research and Development Program of China 2022YFF0802403 (JP)

National Key Research and Development Program of China 2021YFD1800202 (JP)

National Natural Science Foundation of China 32192450 to (JL)

National Natural Science Foundation of China 32102661 (ZJ)

UK Biotechnology and Biological Sciences Research Council BBS/E/D/20002173 (PD and LL)

Author contributions

Research designing: JP, YG

Data collection and analysis: YG, YZ, YL

Experiment: YG, SS, WP, TL, LW, XC, JD, CZ, FD

Funding acquisition: JP, JL, ZJ, PD, LL

Writing – original draft: YG, JP

Writing – review & editing: JL, HLY, LL, PD, KCC, MHW, HS, YS, ZJ, FD

Competing interests

The authors declare that they have no competing interests.

Data and materials availability

Genetic variation data of H9N2 viruses during passage in chickens are available at Zenodo data (DOI: 10.5281/zenodo.12730083). All other data supporting the findings of this study are available in the main text or the supplementary information.

References

1. Krammer F, Smith GJD, Fouchier RAM, Peiris M, Kedzierska K, Doherty PC, et al. Influenza. Nat Rev Dis Primers. 2018;4: 3. doi:10.1038/s41572-018-0002-y

2. Amat JAR, Patton V, Chauché C, Goldfarb D, Crispell J, Gu Q, et al. Long-term adaptation following influenza A virus host shifts results in increased within-host viral fitness due to higher replication rates, broader dissemination within the respiratory epithelium and reduced tissue damage. PLoS Pathog. 2021;17: e1010174. doi:10.1371/journal.ppat.1010174

3. Su W, Harfoot R, Su YCF, DeBeauchamp J, Joseph U, Jayakumar J, et al. Ancestral sequence reconstruction pinpoints adaptations that enable avian influenza virus transmission in pigs. Nat Microbiol. 2021;6: 1455–1465. doi:10.1038/s41564-021-00976-y

4. Wang J, Samaan M. Tool for Influenza Pandemic Risk Assessment - version 2. : 65.

5. European Food Safety Authority, European Centre for Disease Prevention and Control, European Union Reference Laboratory for Avian Influenza, Adlhoch C, Fusaro A, Gonzales JL, Kuiken T, Melidou A, et al. Avian influenza overview April – June 2023. EFS2. 2023;21. doi:10.2903/j.efsa.2023.8191

6. Bi Y, Li J, Shi W. The time is now: a call to contain H9N2 avian influenza viruses. The Lancet Microbe. 2022; S2666524722002324. doi:10.1016/s2666-5247(22)00232-4

7. Koopmans M, Wilbrink B, Conyn M, Natrop G, van der Nat H, Vennema H, et al. Transmission of H7N7 avian influenza A virus to human beings during a large outbreak in commercial poultry farms in the Netherlands. Lancet. 2004;363: 587–593. doi:10.1016/S0140-6736(04)15589-X

8. Pu J, Wang S, Yin Y, Zhang G, Carter RA, Wang J, et al. Evolution of the H9N2 influenza genotype that facilitated the genesis of the novel H7N9 virus. P Natl Acad Sci USA. 2015;112: 548–553. doi:10.1073/pnas.1422456112

9. Pu J, Yin Y, Liu J, Wang X, Zhou Y, Wang Z, et al. Reassortment with Dominant Chicken H9N2 Influenza Virus Contributed to the Fifth H7N9 Virus Human Epidemic. J Virol. 2021;95: e01578-20. doi:10.1128/JVI.01578-20

10. Chen H, Yuan H, Gao R, Zhang J, Wang D, Xiong Y, et al. Clinical and epidemiological characteristics of a fatal case of avian influenza A H10N8 virus infection: a descriptive study. Lancet. 2014;383: 714–721. doi:10.1016/S0140-6736(14)60111-2

11. Bi Y, Chen Q, Wang Q, Chen J, Jin T, Wong G, et al. Genesis, Evolution and Prevalence of H5N6 Avian Influenza Viruses in China. Cell Host & Microbe. 2016;20: 810–821. doi:10.1016/j.chom.2016.10.022

527 12. Qi X, Qiu H, Hao S, Zhu F, Huang Y, Xu K, et al. Human infection with an avian-origin
528 influenza A(H10N3) virus. N Engl J Med. 2022;386: 1087–1088.
529 doi:10.1056/nejmc2112416

530 13. Bao P, Liu Y, Zhang X, Fan H, Zhao J, Mu M, et al. Human infection with a reassortment
531 avian influenza A H3N8 virus: an epidemiological investigation study. Nat Commun.
532 2022;13: 6817. doi:10.1038/s41467-022-34601-1

533 14. Li C, Yu K, Tian G, Yu D, Liu L, Jing B, et al. Evolution of H9N2 influenza viruses from
534 domestic poultry in Mainland China. Virology. 2005;340: 70–83.
535 doi:10.1016/j.virol.2005.06.025

536 15. Peacock TP, James J, Sealy JE, Iqbal M. A global perspective on H9N2 avian influenza virus.
537 Viruses. 2019;11: 620. doi:10.3390/v11070620

538 16. Elgendy EM, Arai Y, Kawashita N, Isobe A, Daidoji T, Ibrahim MS, et al. Double mutations
539 in the H9N2 avian influenza virus PB2 gene act cooperatively to increase viral host adaptation
540 and replication for human infections. Journal of General Virology. 2021;102.
541 doi:10.1099/jgv.0.001612

542 17. Gao Y, Zhang Y, Shinya K, Deng G, Jiang Y, Li Z, et al. Identification of amino acids in HA
543 and PB2 critical for the transmission of H5N1 avian influenza viruses in a mammalian host.
544 PLoS Pathog. 2009;5: e1000709. doi:10.1371/journal.ppat.1000709

545 18. Arai Y, Kawashita N, Hotta K, Hoang PVM, Nguyen HLK, Nguyen TC, et al. Multiple
546 polymerase gene mutations for human adaptation occurring in Asian H5N1 influenza virus
547 clinical isolates. Sci Rep. 2018;8: 13066. doi:10.1038/s41598-018-31397-3

548 19. Zaraket H, Baranovich T, Kaplan BS, Carter R, Song M-S, Paulson JC, et al. Mammalian
549 adaptation of influenza A(H7N9) virus is limited by a narrow genetic bottleneck. Nat
550 Commun. 2015;6: 6553. doi:10.1038/ncomms7553

551 20. Long JS, Mistry B, Haslam SM, Barclay WS. Host and viral determinants of influenza A
552 virus species specificity. Nat Rev Microbiol. 2019;17: 67–81. doi:10.1038/s41579-018-0115-
553 z

554 21. Camacho-Zarco AR, Kalayil S, Maurin D, Salvi N, Delaforge E, Milles S, et al. Molecular
555 basis of host-adaptation interactions between influenza virus polymerase PB2 subunit and
556 ANP32A. Nat Commun. 2020;11: 3656. doi:10.1038/s41467-020-17407-x

557 22. Carrique L, Fan H, Walker AP, Keown JR, Sharps J, Staller E, et al. Host ANP32A mediates
558 the assembly of the influenza virus replicase. Nature. 2020;587: 638–643.
559 doi:10.1038/s41586-020-2927-z

560 23. Long JS, Giotis ES, Moncorgé O, Frise R, Mistry B, James J, et al. Species difference in
561 ANP32A underlies influenza A virus polymerase host restriction. Nature. 2016;529: 101–
562 104. doi:10.1038/nature16474

563 24. Subbarao EK, London W, Murphy BR. A single amino acid in the PB2 gene of influenza A
564 virus is a determinant of host range. J Virol. 1993;67: 1761–1764.

565 25. Zhang H, Zhang Z, Wang Y, Wang M, Wang X, Zhang X, et al. Fundamental contribution
566 and host range determination of ANP32A and ANP32B in influenza A virus polymerase
567 activity. J Virol. 2019;93: e00174-19. doi:10.1128/jvi.00174-19

568 26. Briggs K, Kapczynski DR. Comparative analysis of PB2 residue 627E/K/V in H5 subtypes
569 of avian influenza viruses isolated from birds and mammals. Frontiers in Veterinary Science.
570 2023;10. doi:10.3389/fvets.2023.1250952

571 27. Hatta M, Hatta Y, Kim JH, Watanabe S, Shinya K, Nguyen T, et al. Growth of H5N1
572 influenza A viruses in the upper respiratory tracts of mice. PLoS Pathog. 2007;3: e133.
573 doi:10.1371/journal.ppat.0030133

574 28. Mistry B, Long JS, Schreyer J, Staller E, Sanchez-David RY, Barclay WS. Elucidating the
575 Interactions between Influenza Virus Polymerase and Host Factor ANP32A. J Virol. 2020;94:
576 e01353-19. doi:10.1128/jvi.01353-19

577 29. Braun KM, Moreno GK, Halfmann PJ, Hodcroft EB, Baker DA, Boehm EC, et al.
578 Transmission of SARS-CoV-2 in domestic cats imposes a narrow bottleneck. PLoS Pathog.
579 2021;17: e1009373. doi:10.1371/journal.ppat.1009373

580 30. Moncla LH, Bedford T, Dussart P, Horm SV, Rith S, Buchy P, et al. Quantifying within-host
581 diversity of H5N1 influenza viruses in humans and poultry in Cambodia. PLoS Pathog.
582 2020;16: e1008191. doi:10.1371/journal.ppat.1008191

583 31. Yang R, Sun H, Gao F, Luo K, Huang Z, Tong Q, et al. Human infection of avian influenza
584 a H3N8 virus and the viral origins: a descriptive study. The Lancet Microbe. 2022;3: e824–
585 e834. doi:10.1016/s2666-5247(22)00192-6

586 32. Sun H, Li H, Tong Q, Han Q, Liu J, Yu H, et al. Airborne transmission of human-isolated
587 avian H3N8 influenza virus between ferrets. Cell. 2023;0. doi:10.1016/j.cell.2023.08.011

588 33. Liu WJ, Li J, Zou R, Pan J, Jin T, Li L, et al. Dynamic PB2-E627K substitution of influenza
589 H7N9 virus indicates the in vivo genetic tuning and rapid host adaptation. : 8.
590 doi:10.1073/pnas.2013267117

591 34. Zhu Z, Fodor E, Keown JR. A structural understanding of influenza virus genome replication.
592 Trends in Microbiology. 2023;31: 308–319. doi:10.1016/j.tim.2022.09.015

593 35. Baker SF, Ledwith MP, Mehle A. Differential splicing of ANP32A in birds alters its ability
594 to stimulate rna synthesis by restricted influenza polymerase. Cell Rep. 2018;24: 2581-
595 2588.e4. doi:10.1016/j.celrep.2018.08.012

596 36. Taft AS, Ozawa M, Fitch A, Depasse JV, Halfmann PJ, Hill-Batorski L, et al. Identification
597 of mammalian-adapting mutations in the polymerase complex of an avian H5N1 influenza
598 virus. Nature Communications. 2015;6. doi:10.1038/ncomms8491

599 37. Chin AWH, Li OTW, Mok CKP, Ng MKW, Peiris M, Poon LLM. Influenza A viruses with
600 different amino acid residues at PB2-627 display distinct replication properties in vitro and
601 in vivo: revealing the sequence plasticity of PB2-627 position. Virology. 2014;0: 545–555.
602 doi:10.1016/j.virol.2014.09.008

603 38. Arai Y, Kawashita N, Ibrahim MS, Elgendy EM, Daidoji T, Ono T, et al. PB2 mutations
604 arising during H9N2 influenza evolution in the Middle East confer enhanced replication and
605 growth in mammals. PLoS Pathog. 2019;15: e1007919. doi:10.1371/journal.ppat.1007919

606 39. Li X, Shi J, Guo J, Deng G, Zhang Q, Wang J, et al. Genetics, receptor binding property, and
607 transmissibility in mammals of naturally isolated H9N2 avian influenza viruses. PLoS Pathog.
608 2014;10: e1004508. doi:10.1371/journal.ppat.1004508

609 40. Carnaccini S, Perez DR. H9 influenza viruses: an emerging challenge. Cold Spring Harb
610 Perspect Med. 2020;10: a038588. doi:10.1101/cshperspect.a038588

611 41. Sun X, Belser JA, Maines TR. Adaptation of H9N2 influenza viruses to mammalian hosts: a
612 review of molecular markers. Viruses. 2020;12: 541. doi:10.3390/v12050541

613 42. Sun Y, Pu J, Jiang Z, Guan T, Xia Y, Xu Q, et al. Genotypic evolution and antigenic drift of
614 H9N2 influenza viruses in China from 1994 to 2008. Vet Microbiol. 2010;146: 215–225.
615 doi:10.1016/j.vetmic.2010.05.010

616 43. Xu G, Zhang X, Gao W, Wang C, Wang J, Sun H, et al. Prevailing PA mutation K356R in
617 avian influenza H9N2 virus increases mammalian replication and pathogenicity. Journal of
618 Virology. 2016;90: 8105–8114. doi:10.1128/jvi.00883-16

619 44. Gao W, Zu Z, Liu J, Song J, Wang X, Wang C, et al. Prevailing I292V PB2 mutation in avian
620 influenza H9N2 virus increases viral polymerase function and attenuates IFN-β induction in
621 human cells. J Gen Virol. 2019;100: 1273–1281. doi:10.1099/jgv.0.001294

622 45. Xiao C, Ma W, Sun N, Huang L, Li Y, Zeng Z, et al. PB2-588 V promotes the mammalian
623 adaptation of H10N8, H7N9 and H9N2 avian influenza viruses. Sci Rep-UK. 2016;6: 19474.
624 doi:10.1038/srep19474

625 46. Edgar RC. MUSCLE: a multiple sequence alignment method with reduced time and space
626 complexity. BMC Bioinformatics. 2004;5: 113. doi:10.1186/1471-2105-5-113

627 47. Miller MA, Pfeiffer W, Schwartz T. Creating the cipres science gateway for inference of
628 large phylogenetic trees. 2010 Gateway Computing Environments Workshop (GCE). 2010.
629 pp. 1–8. doi:10.1109/gce.2010.5676129

630 48. Chen C, Wu Y, Li J, Wang X, Zeng Z, Xu J, et al. TBtools-II: A “one for all, all for one”
631 bioinformatics platform for biological big-data mining. Molecular Plant. 2023;16: 1733–
632 1742. doi:10.1016/j.molp.2023.09.010

633 49. Su YCF, Bahl J, Joseph U, Butt KM, Peck HA, Koay ESC, et al. Phylodynamics of
634 H1N1/2009 influenza reveals the transition from host adaptation to immune-driven selection.
635 Nat Commun. 2015;6: 7952. doi:10.1038/ncomms8952

636 50. Hernandez R, Brown DT. Growth and maintenance of chick embryo fibroblasts (CEF). Curr
637 Protoc Microbiol. 2010;Appendix 4: 4I. doi:10.1002/9780471729259.mca04is17

638 51. Zhang P, Tang Y, Liu X, Liu W, Zhang X, Liu H, et al. A novel genotype H9N2 influenza
639 virus possessing human H5N1 internal genomes has been circulating in poultry in eastern
640 china since 1998. J Virol. 2009;83: 8428–8438. doi:10.1128/jvi.00659-09

641 52. Belser JA, Eckert AM, Huynh T, Gary JM, Ritter JM, Tumpey TM, et al. A guide for the use
642 of the ferret model for influenza virus infection. The American Journal of Pathology.
643 2020;190: 11–24. doi:10.1016/j.ajpath.2019.09.017

644
645

646 **Figures and Tables**

647 **Fig 1 Emergence and cross-host species function of PB2-627V.**

648 (**A).** The global prevalence of PB2-627V in influenza A viruses (IAVs) (excluding human H3N2
649 and H1N1pdm09 viruses) during 1994-2022. Bars show the number of isolates by subtype and
650 host, while a world map displays the isolate's number by location. (**B).** Phylogenetic tree of PB2
651 genes with the residue 627V collected worldwide during 1994-2022 (n=394). Human isolates'
652 names are in red. (**C).** Amino acid polymorphisms of the PB2-627 residue in avian and human-
653 derived H9N2 viruses isolated in China. All sequence data were collected from the GISAID
654 database**.** (**D-E)**. Relative polymerase activities at 33°C or 37°C. DF-1 cells **(D)** and 293T cells **(E)**
655 were transfected with firefly minigenome reporter, renilla expression control, and polymerase
656 (PB2, PB1, PA, and NP) of 17/H9N2^{627E}, 17/H9N2^{627V}, or 17/H9N2^{627K}. Cells were incubated for
657 24 hours and the luciferase activities, normalized to corresponding renilla luciferase activity, are
658 presented relative to 17/H9N2^{627E} (set as 1). Each data point is the mean ± SD of three independent
659 experiments (one-way ANOVA). **(F).** Heat map shows p-values of polymerase activities in DKO
660 cells overexpressing ANP32 proteins. chANP32A, chANP32B, huANP32A, huANP32B, or
661 empty vector was transfected into DKO cells, incubated at 33°C and 37°C for 24 hours, and
662 assayed the luciferase activity. Statistical significance was based on one-way ANOVA and
663 subsequent Dunnett's test, compared with the corresponding value of empty vector (ns, not
664 significant; *, $p<0.05$; **, $p<0.01$; ***, $p<0.001$). (**G).** Impact of amino acids at the PB2-627
665 position on the surface charge of the PB2 protein. Red (negative) and blue (positive) proteins are
666 shown.

667 **Fig 2. PB2-627V conferred dual adaptability to H9N2 virus to replicate in avian and**
668 **mammalian species.**

669 (**A).** CEF cells were infected with indicated viruses at 0.01 MOI and virus titers were determined
670 at indicated times post-infection by $TCID_{50}$ assays. (**B-D).** Groups of 6 chickens were i.n. infected
671 with indicated viruses at 10^6 EID_{50}, three chickens from each group were used to determine the
672 viral titers (**B**) from oropharyngeal samplings at 2, 4, 6, and 8 dpi. Another three chickens from
673 each group were euthanized at 3 dpi. Virus titers (**C**) of the turbinates and lungs were determined.
674 Representative histopathological findings (**D**) in the lungs of infected mice. Lung sections were
675 stained with H&E (upper) and by IHC against influenza viral NP antigen (lower). Scale bars, 100
676 mm. (**E).** A549 cells were infected with indicated viruses at 0.1 MOI and virus titers were
677 determined by $TCID_{50}$ assays at indicated times post-infection. (**F-H).** Groups of 8 mice were
678 infected with the indicated virus at doses of 10^6 $TCID_{50}$. Five mice of each group were monitored
679 for body weight changes (**F**) over 14 days. Additional three mice from each group at 3 dpi were
680 euthanized. Virus titers (**G**) in the turbinates and lungs were determined by $TCID_{50}$ assays.
681 Representative histopathological findings (**H**) in the lungs of infected mice. Lung sections were
682 stained with H&E (upper) and by IHC against influenza viral NP antigen (lower). Scale bars, 100
683 mm. Data are represented as mean ± SD. Statistical significance was based on two-way ANOVA,
684 compared with the corresponding value of $17/H9N2^{627E}$ (ns, not significant; *, $p < 0.05$; **, $p <$
685 0.01; ***, $p < 0.001$).

686 **Fig 3 PB2-627V facilitated aerosol transmissibility of H9N2 virus in ferrets.**

687 Each ferret (n = 3) was inoculated with 10^6 $TCID_{50}$ of indicated virus. The next day, the infected
688 ferret was individually paired by co-housing with a DC ferret; an RD-contact ferret was also
689 housed in a wire frame cage adjacent to the infected ferret. Nasal washes were collected for virus-
690 shedding detection every other day from all ferrets from 2 dpi. (**A-C).** Virus titers of nasal washes
691 were determined by $TCID_{50}$ assays on MDCK cells. Each color bar represents virus titers of an

692 individual ferret. Dashed lines indicate the lower limit of virus detection ($10^{1.5}$ $TCID_{50}$/ml). **(D).**
693 AUC values approximate total virus output throughout infection (mean AUC from three ferrets).
694 **(E-G).** For each infected or transmitted ferret, the nasal washes collected at the first and last virus
695 detection time were analyzed by deep sequencing. Detection time points are based on the results
696 shown in Fig. 3, A-C. The height of each letter indicates the relative ratio of amino acids at PB2-
697 627. Sequencing was performed on an Illumina NovaSeq platform.

698 **Fig 4 PB2-627V has the potential for sustained prevalence in poultry.**

699 **(A).** Schematic depiction of virus passage in chickens**.** Groups of 2 chickens were each i.n. infected
700 with 10^6 $TCID_{50}$ of indicated virus (P1), and subsequently passaged (P1-P5) by contact. **(B).** Intra-
701 host single nucleotide variants (iSNVs) frequency of P5 chicken. Variants of nucleotide site
702 detected above 1% threshold were identified as iSNVs. All iSNVs were further determined as
703 high-frequency (>10%) and low-frequency (⩽10%). iSNVs frequency of the whole genome was
704 calculated by using the number of iSNVs divided by the total number of genome sites. iSNVs
705 frequency was expressed as the log. **(C)**. Variant frequency nucleotides encoding PB2-627 residue.
706 The height of each letter indicates the average ratio of nucleotides encoding PB2-627 residue in
707 two samples of each group. **(D)**. Graphs represent all iSNVs detected in P5 chicken. Variant
708 frequencies are plotted by genome location and are colored by virus groups. two high-frequency
709 non-synonymous iSNVs are circled and labeled with the corresponding amino acid mutations.
710 Yellow backgrounds depict RNP genes (PB2, PB1, PA, and NP). Sequencing was performed on
711 an Illumina NovaSeq platform. Data are presented as mean ± SD. Statistical significance was based
712 on two-way ANOVA (ns, not significant, *, $p < 0.05$; **, $p < 0.01$; ***, $p < 0.001$).

713 **Fig 5 PB2-627V conferred dual adaptability in avian H7N9 and H3N8 viruses to replicate in**
714 **chickens and mice.**

715 **(A-E).** Groups of 6 chickens were infected with indicated viruses at doses of 10^6 EID_{50}. Three
716 infected chickens in each group were monitored for survival (**A**, **C)** over 14 days. At 3 dpi, the
717 other three chickens in each group were euthanized. Virus titers (**B**, **D**) in the turbinates and lungs
718 were determined by $TCID_{50}$ assays. Representative histopathological findings (**E**) in the lungs of
719 infected mice. Lung sections were stained with H&E (left) and by IHC against influenza viral NP
720 antigen (right). Scale bars, 100 mm. (**F-L).** Groups of 8 mice were infected with indicated viruses
721 at doses of 10^6 $TCID_{50}$. Five mice in each group were monitored for survival (**F**, **I**) and body weight
722 changes (**G**, **J**) over 14 days. Mortality from infection included mice euthanized at a weight loss
723 of 25% or more. At 3 dpi, the other three mice in each group were euthanized. Virus titers (**H**, **K**)
724 in the turbinates and lungs were determined by $TCID_{50}$ assays. Representative histopathological
725 findings (**L**) in the lungs of infected mice. Lung sections were stained with H&E (left) and by IHC
726 against influenza viral NP antigen (right). Scale bars, 100 mm. Data presented are represented as
727 mean ± SD. Statistical significance was based on two-way ANOVA (ns, not significant; *, $p <$
728 0.05; **, $p < 0.01$; ***, $p < 0.001$).

729 # Supporting information

730 **S1 Fig. H9N2 virus and its reassortants with PB2-627V are in the same cluster. (A).** A total
731 of 4523 H9N2 PB2 sequences were collected from GISAID, Amino acid at PB2-627 residue and
732 the location of all isolates are shown. **(B).** The MCC tree of the PB2-627V cluster. The internal
733 nodes indicated the most recent common ancestor of the sub-group, which is divided into avian
734 and human. All human strains' names are in bold.

735 **S2 Fig. Increased detection of PB2-627V in novel AIVs reassortant with H9N2 PB2 gene since**
736 **2016.** All the sequences of H7N9, H5N6, H10N3 and H3N8 PB2 genes were obtained from the
737 GISAID database. Viruses with PB2 gene identity greater than 97% to that of PB2 gene of H9N2

738 viruses were considered reassortants of H9N2. The bars depict the number of isolates with PB2-
739 627V in different subtypes and hosts before and after 2016.

740 **S3 Fig. Host ANP32 required for viral polymerase and differential viral RNA production in**
741 **avian and human cells. (A, B).** DF-1 cells **(A)** and A549 cells **(B)** were infected with indicated
742 viruses at MOI of 0.001 and 0.1 respectively. The cells were cultured at 37°C for 24 hours after
743 infection. PB2 mRNA and vRNA, normalized to β-actin expression, determined by quantitative
744 real-time PCR. **(C).** Wild-type 293T cells and DKO cells were transfected with firefly minigenome
745 reporter, renilla expression control, and polymerase genes of 17/H9N2^{627E}, 17/H9N2^{627V}, or
746 17/H9N2^{627K}. The cells were cultured at 37°C for 24 hours after transfection. Data indicate the
747 firefly luciferase gene activity normalized to the renilla luciferase gene activity. Statistical
748 differences between samples are indicated, based on one-way ANOVA with Dunnett's testing (ns,
749 not significant; *, $p < 0.05$; **, $p < 0.01$; ***, $p < 0.001$). Error bars are SEM in one representative
750 experiment.

751 **S4 Fig. Survival of infected mice and chickens. (A)**. Groups of 3 chickens were i.n. infected
752 with indicated viruses at 10^6 EID_{50}, and the survival were monitored for 14 days. **(B).** Groups of
753 5 mice were infected with indicated virus at doses of 10^6 $TCID_{50}$ and the survival were monitored
754 for 14 days.

755 **S5 Fig. H&E and IHC of chicken and mouse lungs infected with PB2-627 variant H3N8**
756 **viruses. (A).** Chickens were infected at 10^6 EID_{50} with indicated viruses, and three chickens per
757 group were euthanized at 3 dpi. **(B).** Mice were infected at 10^6 $TCID_{50}$ with indicated viruses, and
758 three mice per group were euthanized at 3 dpi. Lung sections were stained with H&E and subjected
759 IHC for the detection of viral NP protein. Scale bars, 100 μm.

760 **S1 Table. Hosts, geographical distribution, and subtypes of AIVs carrying PB2-627V.**

761 **S2 Table. Clinical symptoms of ferrets infected with H9N2 influenza viruses**

762 **S3 Table. Area under the curve (AUC) values of virus output of infected/exposed ferrets**

763

764

765

766

767

768

769

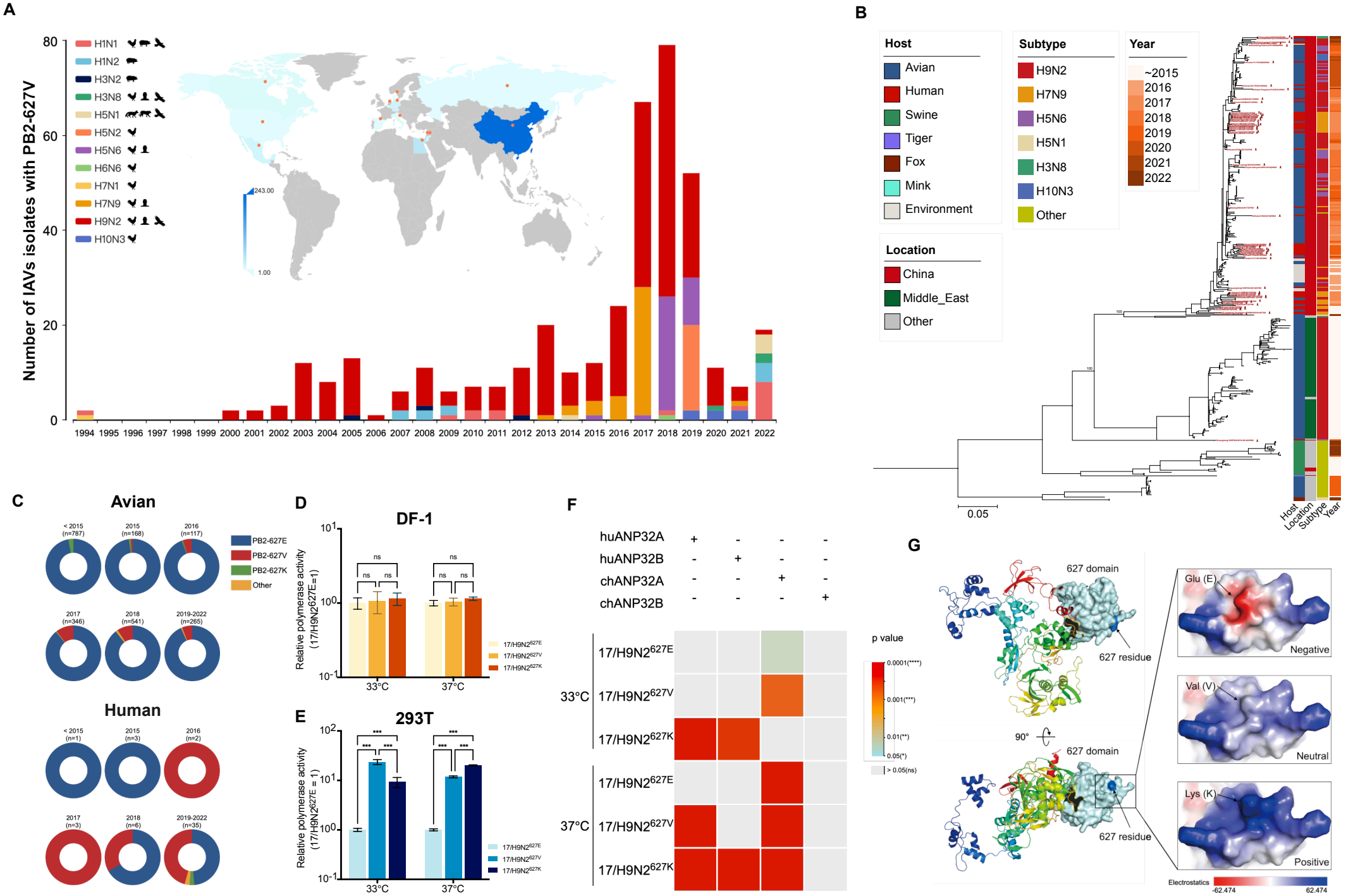

Fig 1. Emergence and cross-host polymerase activity of PB2-627V

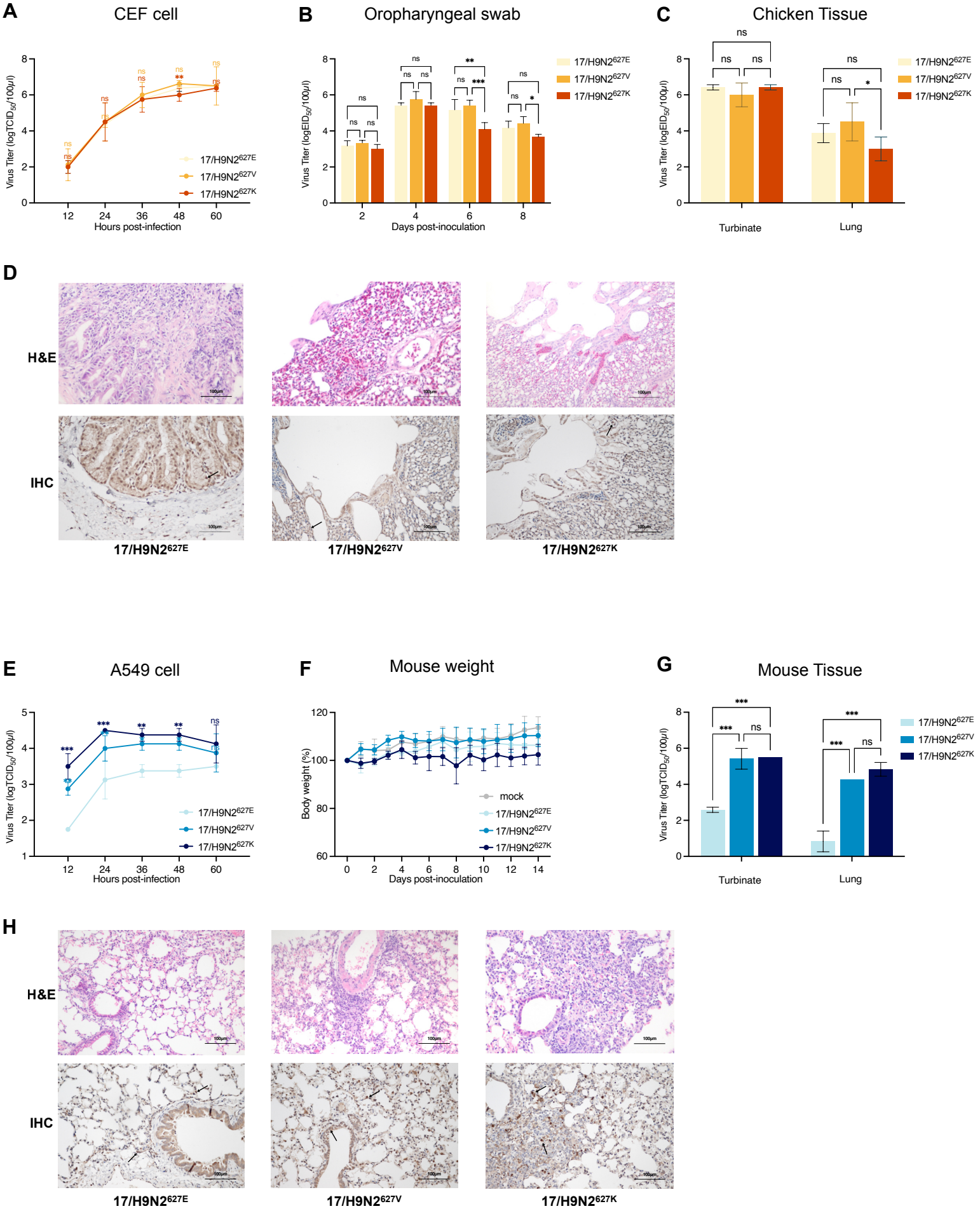

Fig 2. PB2-627V conferred dual adaptability to H9N2 virus to replicate in avian and mammalian species.

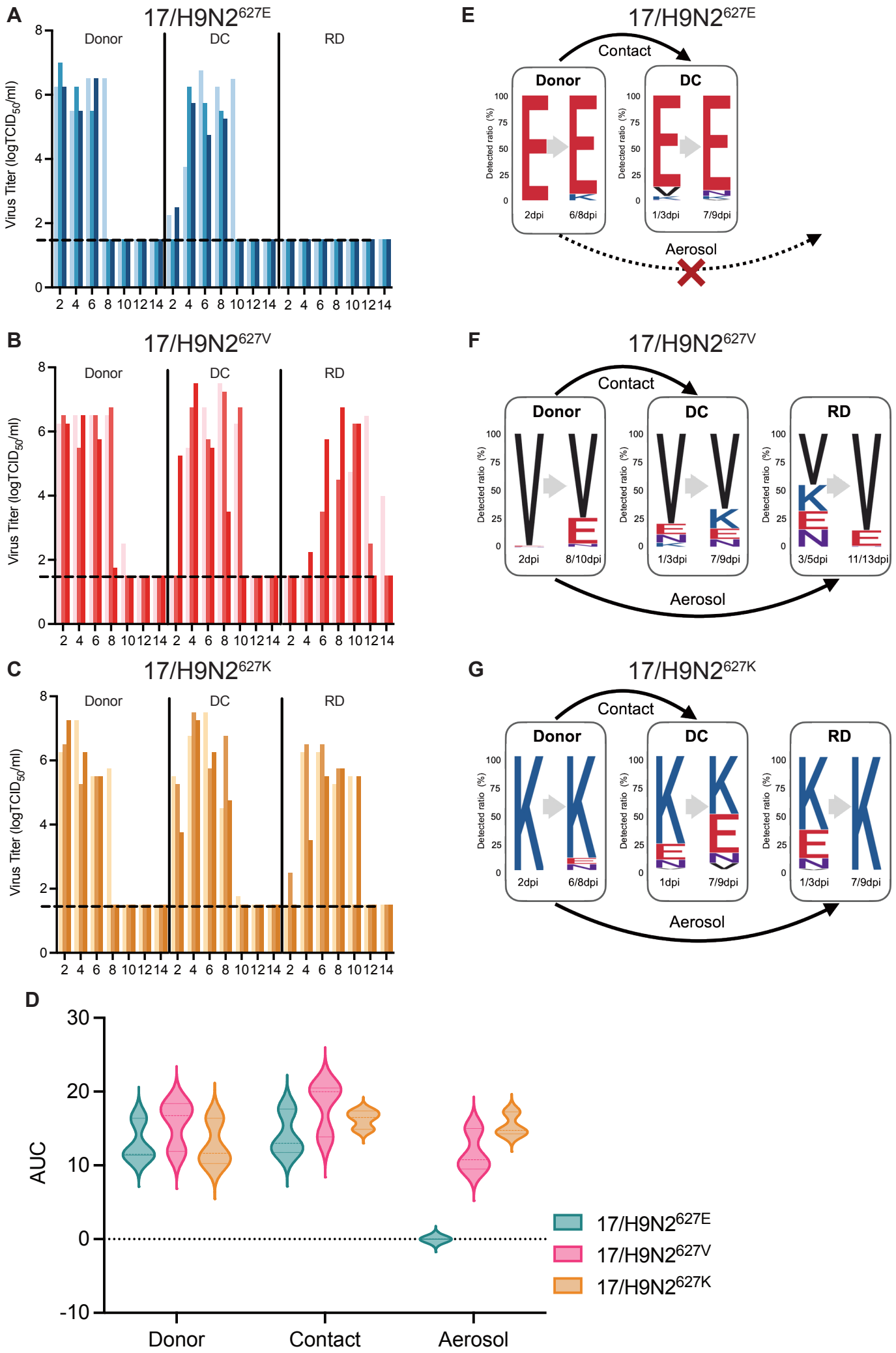

Fig 3. PB2-627V facilitated aerosol transmissibility of H9N2 virus in ferrets

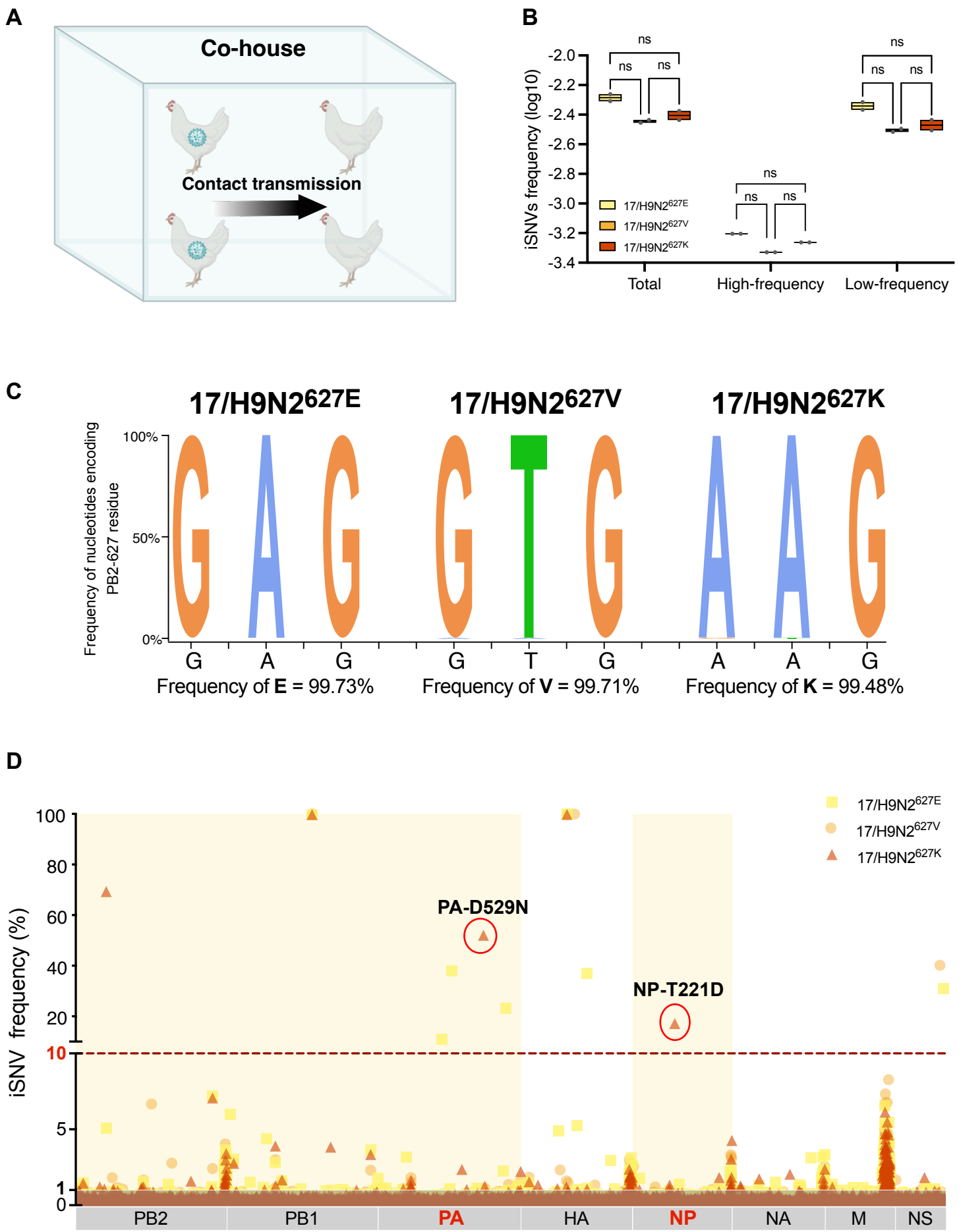

Fig 4. PB2-627V has the potential for sustained prevalence in poultry

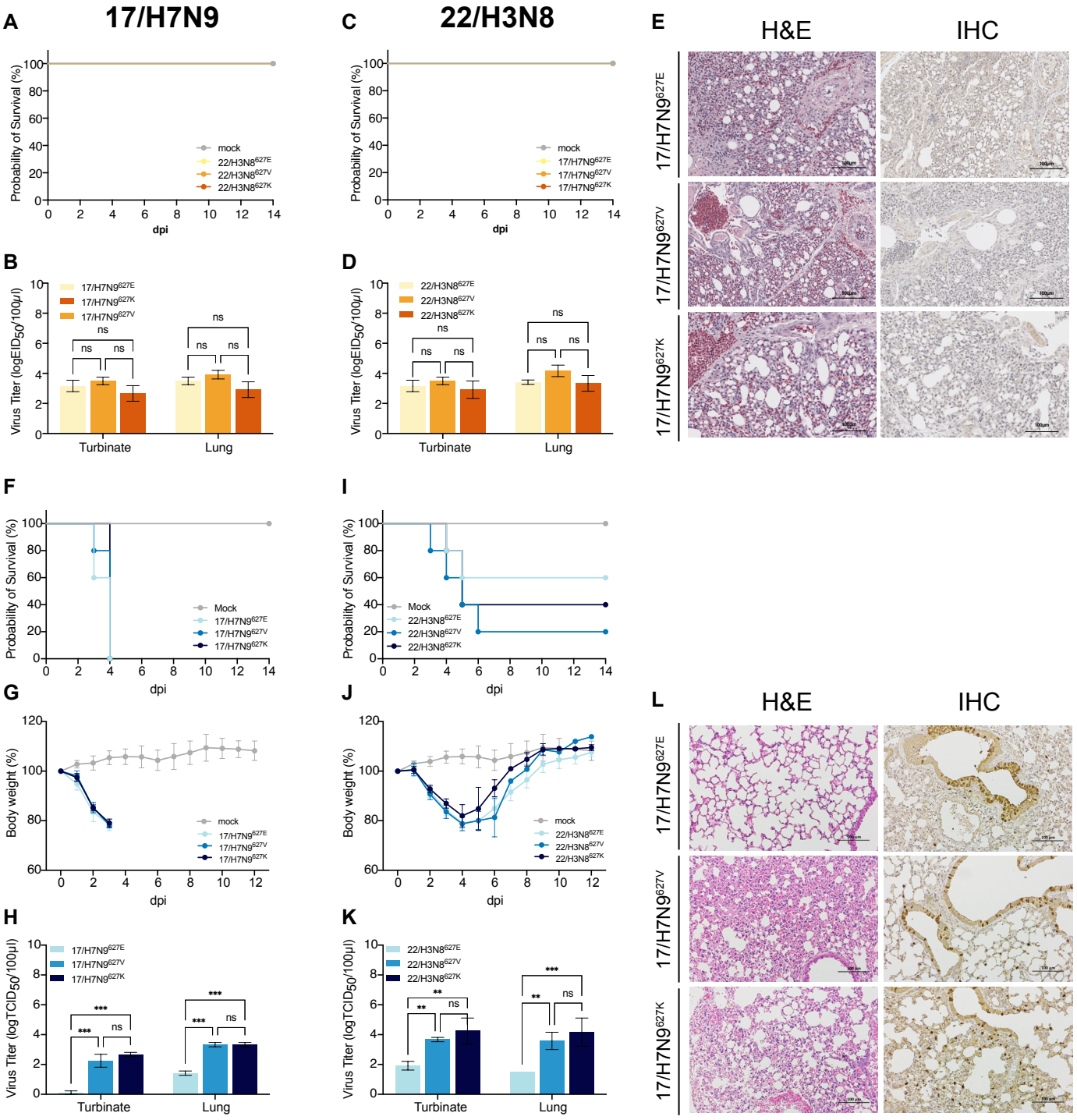

Fig 5. PB2-627V conferred dual adaptability in avian H7N9 and H3N8 viruses to replicate in chickens and mice